An unexpected signature of Lorenz-Mie scattering observed in FlowCytometric experiments

Alfons G. Hoekstra,* Richard M.P. Doornbos,** Kirsten E.I. Deurloo,**
Herke Jan. Noordmans,** Bart G. de Grooth,** and Peter M.A. Sloot*

* Faculty of Mathematics and Computer Science, University of Amsterdam,

Kruislaan 403, 1098 SJ Amsterdam, the Netherlands, tel. (+31)20-5257463

** Faculty of Applied Physics, University of Twente, P.O. Box 217, 7500 AE Enschede,

the Netherlands

Published in
Proceedings of the 3rd International Congress on Optical Particle Sizing '93 (M. Maeda, ed.), (Yokohama, Japan), pp. 153-158, August 23-26 1993.

Abstract

Detailed analysis of elastic light scattering by spheres in FlowCytometers shows unexpected Lorenz-Mie scattering patterns. The complete scattering matrix **S** of spheres was measured. Two parameter scatterplots with x- and y- coordinates determined by the $\mathbf{S}_{11} + \mathbf{S}_{ij}$ and $\mathbf{S}_{11} - \mathbf{S}_{ij}$ values were obtained. Samples of spheres with very narrow size distributions were analyzed and produced unexpected two parameter scatterplots. Instead of compact distributions we observed Lissajous-like loops. Simulation of the scatterplots, using Lorenz-Mie theory, shows that these loops are not due to experimental errors, but due to true Lorenz-Mie scattering. We show that the loops originate from the sensitivity of the scattered field on the radius of the spheres. This work demonstrates that the interpretation of rare events and hidden features in FlowCytometry needs reconsideration.

1 Introduction

The problem of scattering of electromagnetic plane waves by an isotropic, homogeneous sphere of arbitrary size and refractive index was solved in 1890 by Lorenz [1]. Eighteen years later Mie, independent of Lorenz, arrived at the same, exact, analytical solution [2]. The Lorenz-Mie scattering formula posses some remarkable properties. Well-known examples are the interference and ripple structure of the extinction cross section [e.g. 3], glare points [e.g. 4], or rainbows and glories [e.g. 5, 6]

Here we report on yet another face of Lorenz-Mie scattering, which is based on the extreme sensitivity of the scattered field on the radius of the sphere. We measure the total scattering matrix of spheres with a narrow size distribution ($\Delta r/r \sim 1$ %, with r the radius of the sphere) in a dedicated FlowCytometer (FCM). This experimental equipment allows us to measure $\mathbf{S}_{11}+\mathbf{S}_{ij}$ and $\mathbf{S}_{11}-\mathbf{S}_{ij}$ (ij = 12, 33, 34, **S** is the 4×4 scattering matrix) simultaneously for every single sphere in the distribution. FlowCytometry data is usually analyzed by generating a N-dimensional histogram (N being the number of observables per particle, here N = 2) from the experimental data and trying to identify different dataclusters in the histogram with different particles in the sample [7]. At first sight a distribution of homogeneous spheres with a very narrow Gaussian size distribution is expected to produce a single, narrow, Gaussian-like 2-dimensional histogram. However, it turned out that the measured histograms are all but Gaussian; we measure Lissajous-like loops.

2 Materials and Methods

2.1 FlowCytometry

FlowCytometry [7] is an important technique in the biological sciences to identify and separate various populations of e.g. white bloodcells. Hydrodynamic focussing forces the cells to flow through a focussed laser beam one by one. Usually the cells are stained with fluorescent probes and the fluorescence of a cell in the laser beam is measured. Furthermore, the forward - and sideward scattered light is used as an important additional parameter for the analysis. In this way we can

measure several fluorescence and elastic light scattering (ELS) signals for each cell in the sample.

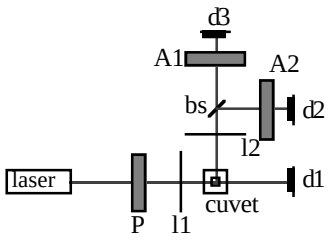

Figure 1: Schematic drawing of the optical system of the FlowCytometer. The laser beam is focussed by lens **l1** on a cell, flowing through the cuvet. The incident beam is polarized by means of the polarizer **P**. The intensity of the forward scattered light is measured by detector **d1**, the sideward scattered light is focussed by lens **l2** on detectors **d2** and **d3**, **bs** is a beamsplitter. The side scattering signals are passed through two different analyzers **A1** and **A2**.

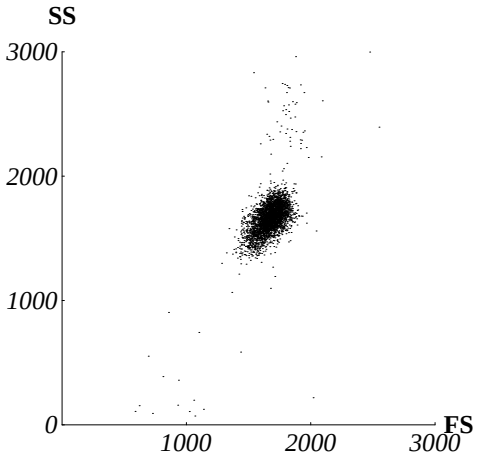

Figure 2: An example of a two parameter scatterplot for a large number of polystyrene spheres with a mean diameter of 1.98 μm, measured with a FlowCytometer. The wavelength was 0.6328 μm. Every dot represents a single sphere, the value of the x-coordinate is the intensity of the forward scattered light, the value of the y-coordinate is the intensity of the sideward scattered light. The intensities are in arbitrary units.

We developed optics to measure the total scattering matrix in a FlowCytometer and showed that quantitative determination of the scattering matrix elements of particles in flow is possible [8,9]. The measuring principle was straightforward: a polarizer P was situated in the incident beam and an analyzer A just before a detector in one of the principal directions. The matrix elements are obtained by measuring scattered intensities for various P-A combinations. We have extended the optics to allow simultaneous measurement of two P-A combinations in the side scattering direction, see figure 1. Figure 2 shows an example of a scatterplot of the Forward and Sideward scattered light of a sample of 1.98 μm polystyrene spheres.

2.2 Polystyrene spheres

The experiments were performed with polystyrene microspheres from Duke Scientific.* The diameters of the spheres are 1.98±0.05 μm, and 7.04±0.05 μm.
In addition to the diameter of the sphere, Lorenz-Mie calculations require the relative refractive index of the sphere. The refractive index of distiled water, in which the spheres are suspended, and polystyrene can be calculated from [10]:

$$n_{water} = n_0 + {}^{n_2}\!/_{\lambda^2} + {}^{n_4}\!/_{\lambda^4} \ , \qquad [1]$$

with λ in micrometers, and n_0 = 1.3236, n_2 = 3.35×10^{-3}, and n_4 = -3.45×10^{-5} for water, and n_0 = 1.5711, n_2 = 4.82×10^{-3}, and n_4 = 6.78×10^{-4} for polystyrene. In our case λ = 0.6328 μm, which gives n_{water} = 1.3318 and $n_{polystyrene}$ = 1.5874. In the calculations we will use

$$n_{relative} = n_{polystyrene} / n_{water} = 1.192,$$

and diameters as reported above.

2.3 Simulation of the scatterplots

To simulate the two parameter scatterplots the intensities measured by the sideward detectors must be calculated. For spheres, using the P-A combinations as described by Sloot et al., the intensity of the scattered light after analyzer A1 and A2 is [8]

$$I_A = I_0\, C\, (\mathbf{S}_{11} \pm \mathbf{S}_{ij}),\ ij = 12,\ 33,\ \text{or}\ 34, \qquad [2]$$

with I_0 the intensity of the laser beam, C an apparatus constant, and **S** the 4×4 scattering matrix of the sphere. The total intensity on the detector is obtained by integrating over the full solid angle dΩ defined by the field of view of the objective,

$$\begin{aligned} I_{det} &= \int_{d\omega} I_A\, d\omega = I_0\, C \left(\int_{d\omega} \mathbf{S}_{11} d\omega \pm \int_{d\omega} \mathbf{S}_{ij} d\omega \right) \\ &\equiv I_0 C \left(\mathbf{s}_{11} \pm \mathbf{s}_{ij} \right) \end{aligned} \ , \qquad [3]$$

with $\mathbf{s}_{ij}$ an integrated matrix element.
To calculate the scattering matrix of a sphere in a focussed laser beam, the traditional Lorenz-Mie theory cannot be applied. Here we must rely on the generalized Lorenz-Mie theory which describes the scattering of a sphere in a Gaussian beam [11]. The $\mathbf{g}_n$ coefficients

* Duke Scientific Polystyrene microspheres 1135D. San Antonio Palo Alto CA 94303

appearing in this theory are calculated using the localized interpretation [12, 13] We use the same programs as described in reference [8]. The beamwaist radius of the Gaussian beam is 12.5 μm (see section 2.1). The particles are located in the focal point of the beam.

The procedure to generate a simulated scatterplot is as follows. First we calculate the scattering matrix $\mathbf{S}(\theta)$ as a function of the scattering angle θ (resolution $d\theta$ = 0.1˚) for a sphere with relative refractive index 1.192, diameter d, wavelength of the incident light 0.6328 μm, and the appropriate beamwaist diameter. Then the integrated scattering elements $\mathbf{s}_{ij}$ are calculated, as described in reference [8]. The $\mathbf{s}_{ij}$ are calculated for 500 different values of d in the range

$$d_{mean} - 4\sigma_d \le d \le d_{mean} + 4\sigma_d \,, \qquad [4]$$

d_{mean} is the mean diameter in the distribution and σ_d the standard deviation (assuming a normal distribution in diameter). This results in arrays of $\mathbf{s}_{ij}(d_i)$, with discrete values d_i as defined above. For every d_i the $\mathbf{s}_{ij}(d_i)$ determine coordinates of a dot in the two parameter scatterplot, and the total scatterplot is generated by drawing dots for every value of d_i.

2.4 Comparison between theory and experiment

The result of the calculations is a set $(\mathbf{s}_{11}, \mathbf{s}_{12}, \mathbf{s}_{33}, \mathbf{s}_{34})_i$, i runs over all the values of d. The measurements give arrays of detector signals, as in formula 3. We need an independent scaling for both theory and experiment in order to compare the two. The experimental results are scaled such that the apparatus constants I_0 and C are removed and the experimental scatterplots are entirely described in terms of scattering matrix elements. The scaling factor for the experimental results is

$$\text{scale}_{exp} = \frac{1}{2p}\sum_{i=1}^{p}(I_{A1}^{i} + I_{A2}^{i}) = \frac{1}{2p}\sum_{i=1}^{p}\mathbf{s}_{11}^{i} \,, \qquad [5]$$

with p the total number of measured spheres, and I_{A1} and I_{A2} the intensities of the scattered light after analyzer A1 and A2. Dividing the measurements by this factor results in two parameters for each measured sphere, independent of I_0 and C:

$$\left(\frac{1}{p}\sum_{i=1}^{p}\mathbf{s}_{11}^{i}\right)^{-1}(\mathbf{s}_{11} \pm \mathbf{s}_{ij}) \,. \qquad [6]$$

These normalized experimental parameters are used as (x,y) coordinates in the scatterplots.

The term

$$\frac{1}{p}\sum_{i=1}^{p}\mathbf{s}_{11}^{i}$$

is the weighted mean $\mathbf{s}_{11}$ of the distribution of spheres. Assuming a normal distribution in diameter, this term is easily calculated from theory:

$$\bar{\mathbf{s}}_{11} = \int_0^{\infty} \frac{1}{\sigma_d\sqrt{2\pi}} \exp\left[-\left(d - d_{mean}\right)^2 \; 2\sigma_d^2\right]\mathbf{s}_{11}(d)\delta d \,. \qquad [7]$$

This integral is approximated by numerical evaluation for $d_{mean} - 4\sigma_d \le d \le d_{mean} + 4\sigma_d$, using Simpson's rule. The calculated integrated scattering matrix elements are divided by the value of this integral. After scaling, both theory and experiment can be compared. In the sequel of this paper the scatterplots of experimental and theoretical data are always scaled accordingly.

3 Results

We measured $(\mathbf{s}_{11}+\mathbf{s}_{ij}, \mathbf{s}_{11}-\mathbf{s}_{ij})$ scatterplots for polystyrene spheres, with a diameter of 7.04 ± 0.05 μm and a diameter of 1.98 ± 0.05 μm, where $\mathbf{s}_{ij}$ is a matrix element integrated over the field of view of the side scattering detectors. Furthermore we simulated the scatterplots using generalized Lorenz-Mie theory. The experimental and theoretical scatterplots were normalized independently to allow for a comparison. Figure 3 and 4 show the normalized theoretical and experimental $(\mathbf{s}_{11}+\mathbf{s}_{12}, \mathbf{s}_{11}-\mathbf{s}_{12})$ scatterplot for the 7.04 μm and the 1.98 μm spheres respectively. The results for the other matrix elements will be published elsewhere.

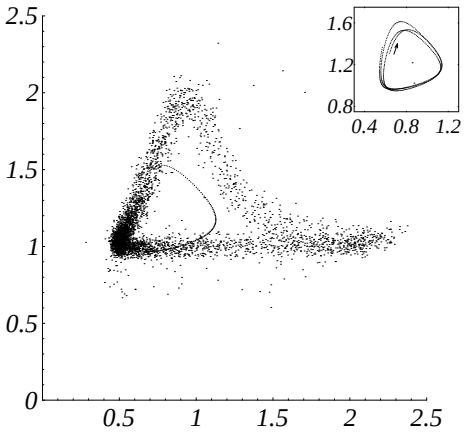

Figure 3: The normalized experimental and theoretical $(\mathbf{s}_{11}+\mathbf{s}_{12}, \mathbf{s}_{11}-\mathbf{s}_{12})$ scatterplot for polystyrene spheres with a mean diameter of 7.04 μm. The horizontal axes is the $\mathbf{s}_{11}+\mathbf{s}_{12}$ signal in the sideward direction, the vertical axes is the $\mathbf{s}_{11}-\mathbf{s}_{12}$ signal in the sideward direction. The inset shows the theoretical curve only, without scaling of the dot diameter. The arrow represents the starting point ($d_i = d_{mean} - 4\sigma_d$) and the loop direction, as d_i grows, of the theoretical curve.

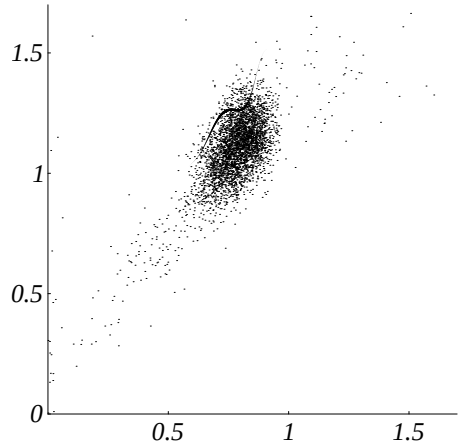

Figure 4: The normalized experimental and theoretical ($\mathbf{s}_{11}+\mathbf{s}_{12}$, $\mathbf{s}_{11}-\mathbf{s}_{12}$) scatterplot for polystyrene spheres with a mean diameter of 1.98 μm. The horizontal axes is the $\mathbf{s}_{11}+\mathbf{s}_{12}$ signal in the sideward direction, the vertical axes is the $\mathbf{s}_{11}-\mathbf{s}_{12}$ signal in the sideward direction.

4 DISCUSSION

Figure 3 shows a loop; theory and experiment agree very well. This demonstrates that the observed loops in the experimental plots are due to Lorenz-Mie scattering, and cannot be attributed to optical misalignments or other experimental errors. The occurrence of loops in the scatterplots however depends on the diameter of the spheres. Figure 4 shows a dense distribution of points, again in agreement with the theoretical results.

We have carried out additional experiments which all are in agreement with the calculations. We measured the scatterplots for a slightly larger wavelength of the incident light (λ = 647 nm). In that case one expects that the same experimental loops occur, but with a small shift of the distribution of the data points in the loop. We indeed observed this shift of the data points. Furthermore we were able to locate particles with larger and smaller forward scattered intensities in different parts of the loop of figure 3, as expected by theory.

The origin of the loops in the scatterplots can be understood by examining the integrated matrix elements as a function of the diameter of the sphere. Figure 5 plots $\mathbf{s}_{11}$, $\mathbf{s}_{12}$, $\mathbf{s}_{33}$, and $\mathbf{s}_{34}$ as a function of the diameter of the sphere, for d as in equation 4, and d_{mean} is 7.04 μm. The matrix elements posses an extreme sensitivity on the diameter of the sphere. For 6.84 μm < d < 7.24 μm, $\mathbf{s}_{11}$ goes through three minima and maxima. The amplitude of the oscillations is approximately 20% of the mean value of $\mathbf{s}_{11}$. The other integrated scattering matrix elements have the same properties, although the oscillations are not in phase with the $\mathbf{s}_{11}$ oscillations. However, for spheres with 1.78 μm < d < 2.18 μm the $\mathbf{s}_{ij}$ elements increase monotonously with increasing d (data not shown).

In the diameter range of figure 5 the integrated scattering functions are almost periodic. The $\mathbf{s}_{11}$ strongly resembles a sine function. The other (quasi) periodic scattering matrix elements can be viewed as a Fourier series of sine and cosine functions. Fourier transformation of the data in figure 5 supports this view. For all four scattering matrix elements the absolute value of the Fourier transform peaks around the same ground frequency ν_0, and around higher harmonics $k\nu_0$ (with k an integer > 1). The amplitude of the third and higher harmonics are negligible compared to the amplitude of the ground frequency (data not shown).

When constructing the theoretical scatterplot, we actually draw a parametric plot, with the diameter of the sphere d as the only parameter. The functions on the x - and y-axes of the scatterplot are approximately combinations of sines and cosines of some ground frequency and higher harmonics. Therefore the scatterplots can be viewed as Lissajous plots. The oscillations in the integrated matrix elements, which are not in phase with each other, give rise to the Lissajous loops in the two parameter scatterplots. Note that in principle it is possible to measure more complicated scatterplots, with e.g. double loops (a ground frequency oscillation in one direction and a first harmonic oscillation in the other direction). Actually, in one instance we measured scatterplots with such double loops. We are still working on the interpretation of these experiments.

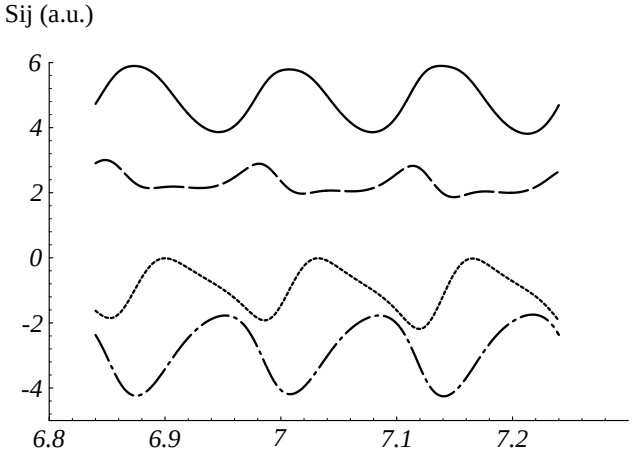

Figure 5: The integrated scattering matrix elements, as a function of the diameter d of the sphere; d is in micrometer, the $\mathbf{s}_{ij}$ are in arbitrary units; the solid line is $\mathbf{s}_{11}$; the dotted line is $\mathbf{s}_{12}$; the dashed line is $\mathbf{s}_{33}$; the dashed-dotted line is $\mathbf{s}_{34}$.

Measurement of polarized light scattering in FCM is by no means a routine procedure yet, nevertheless our results contain an important warning. It is common practice in FCM to measure a side scattering signal. Since the incident light is always linearly polarized (most lasers emit light which is linearly polarized,

perpendicular to the scattering plane), the intensity on the side scattering detectors is always a combination of $\mathbf{s}_{11}$ and $\mathbf{s}_{12}$. Therefore a narrow monodisperse distribution of spheres can produce bimodal histograms in the side scattering channels (this can be seen in figure 3 for the $\mathbf{s}_{11} + \mathbf{s}_{12}$ signal). Especially if spheres are applied to calibrate the instrument, extra care should be taken, and small spheres should be used to avoid the above mentioned problems. Furthermore, interpretation of rare events and hidden distributions in scatterplots requires careful analysis in view of the above mentioned effect. We are currently investigating to which extent the Lissajous loops can be expected in scatterplots from biological particles.

5 CONCLUSIONS

This report shows yet another face of Lorenz-Mie scattering; unexpected, Lissajous-like loops in two parameter scatterplots of spheres, as obtained by FlowCytometry. By simulating the scatterplots, it was shown that the experimental results are true Lorenz-Mie scattering phenomena, and not due to experimental errors. The occurrence of loops in the scatterplots is dependent on the diameter of the spheres. It was shown that oscillations in the integrated matrix elements, as a function of the diameter of the sphere, form the basis for the Lissajous loops.

A consequence of this behaviour is the origin of bimodal histograms in the side scattering channels, due to monodisperse samples. This will hamper the interpretation of rare events and hidden distributions in the scatterplots.

6 ACKNOWLEDGEMENTS

We greatly acknowledge financial support from the Netherlands Organization for Scientific Research, via a matched funding from "FOM", "SION", and "foundation for Biophysics", grant number NWO 810-410-04 1.

7 REFERENCES

[1] L.V. Lorenz: Upon the light reflected and refracted by a transparant sphere. Vidensk. Selsk. Shrifter *6* (1890) 1-62.

[2] G. Mie: Considerations on the optics of turbid media, especially colloidal metal sols. Ann. d. Physik *25* (1908) 377-442.

[3] C.F. Bohren, D.R. Huffman: Absorption and Scattering of Light by Small Particles. John Wiley & Sons 1983.

[4] H.C. van de Hulst, R. Wang: Glare Point. Applied Optics *30* (1991) 4755-6763.

[5] R.T. Wang, H.C. van de Hulst: Rainbows: Mie computations and the Airy approximation. Applied Optics *30* (1991) 106-117.

[6] H.M. Nussenzveig: Complex angular momentum theory of the rainbow and the glory. J. Opt. Soc. Am. *69* (1979) 1068-1079.

[7] M.A. van Dilla, P.N. Dean, O.D. Laerum, M.R. Melamed: Flow Cytometry: Instrumentation and Data Analysis. Academic Press 1985.

[8] P.M.A. Sloot, A.G. Hoekstra, H. van der Liet, C.G. Figdor: Scattering matrix elements of biological particles measured in a flow through system: theory and practice. Applied Optics *28* (1989) 1752-1762.

[9] P.M.A. Sloot, A.G. Hoekstra: Arbitrary-shaped particles measured in flow through systems, in E.D. Hirleman (eds.)Proceedings of the 2nd international congress on optical particle sizing: Vol. . 1990.

[10] E. Gulari: Latex particle size distributions from multiwavelength turbidity spectra. Part. Charact. *4* (1987) 96.

[11] G. Gouesbet, B. Maheu, G. Grehan: Light scattering from a sphere arbitrary located in a Gaussian beam, using a Bromwich formulation. J. Opt. Soc. Am. A *5* (1988) 1427-1443.

[12] G. Grehan, B. Maheu, G. Gouesbet: Scattering of laser beams by Mie scatter centers: numerical results using a localized approximation. Applied Optics *25* (1986) 3539-3548.

[13] G. Gouesbet, G. Gréhan, B. Maheu: Localized interpretation to compute all the coefficients g(n,m) in the generalized Lorenz-Mie theory. J. Opt. Soc. Am. A *7* (1990) 998-1007.